Efficient Operation of a High-Power X-Band Gyroklystron

W. Lawson, J. P. Calame, B. Hogan, P. E. Latham, M. E. Read,[a] V. L. Granatstein, M. Reiser, and C. D. Striffler

Laboratory for Plasma Research and Electrical Engineering Department, University of Maryland, College Park, Maryland 20742

(Received 25 February 1991)

Experimental studies of amplification in a two-cavity X-band gyroklystron are reported. The system utilizes a thermionic magnetron injection gun at voltages up to 440 kV and currents up to 190 A in 1-μs pulses. Optimum performance is achieved by tapering the magnetic-field profile. Peak powers of 20 MW in the TE_{01} mode at 9.87 GHz are measured with calibrated crystals and with methanol calorimetry. Resultant efficiencies are in excess of 31% and large-signal gains surpass 26 dB. The experimental results are in good agreement with simulated results from a partially self-consistent, nonlinear, steady-state code.

PACS numbers: 85.10.Jz, 41.80.Ee

An international effort is under way to develop high-power microwave amplifiers in the 10–20-GHz frequency range for driving future electron-positron colliders operating at multi-TeV energies [1]. Much of the research is centered on extending the frequency and power capabilities of "conventional" klystrons [2], but limits in this approach have been reached in part because of electrical breakdown in the gap of the klystron output cavity. This paper reports initial success in operating a gyrotron amplifier with output power of tens of megawatts. The gyrotron is based on the relativistic cyclotron instability [3] and can operate with overmoded cylindrical (gapless) cavities. Thus, it should scale more favorably to the frequencies and powers desired for the TeV linear colliders [4].

The gyrotron has proven to be an efficient, high-power, high-frequency oscillator [5]. For example [6,7], peak powers near 1 MW with microsecond pulse durations have been achieved at high frequencies ($\sim$140 GHz) in highly overmoded cavities. Recent gyrotron amplifier experiments have included gyrotron traveling-wave tubes [8] and gyroklystrons [9,10]. Overmoded gyroklystrons have had considerable difficulties due to spurious oscillations in regions outside of the cavities. Peak powers in low-voltage gyroklystrons (<100 kV) have remained near 50 kW.

Our present effort to increase gyroklystron power levels has focused on two issues. The first involves increasing the beam voltage above conventional (long pulse) levels as described in previous design papers [11,12]. Toward this goal, a double-anode magnetron injection gun (MIG) was developed [13] that is capable of producing a high-quality, 500-kV, 200-A beam with a ratio of perpendicular to parallel velocity ($v_\perp/v_z$) of $\alpha=1.5$. The second issue involves the development of suitable microwave absorber configurations to improve stability. For this effort, a procedure to carbonize aluminum silicate was modified to improve sample reliability [14]. In this paper, we briefly describe the experimental configuration, discuss the microwave diagnostics, and present optimal two-cavity gyroklystron performance. Details of the experimental setup, tube stability, and flat-field amplifier experiments that achieved peak powers of 2.7 MW appear elsewhere [15].

A schematic of the overall system is shown in Fig. 1(a). A 1.5-μs, 500-kV, 400-A line-type modulator provides the required voltages to the MIG. Eight water-cooled coils are powered by four independent supplies and can produce peak magnetic fields of 0.7 T. This arrangement allows great flexibility in producing linear variations in the magnetic-field strength. The nominal flat field is 0.565 T and the nominal magnetic compression of 12 occurs over a distance of 0.4825 m. A 2-μs, 100-kW

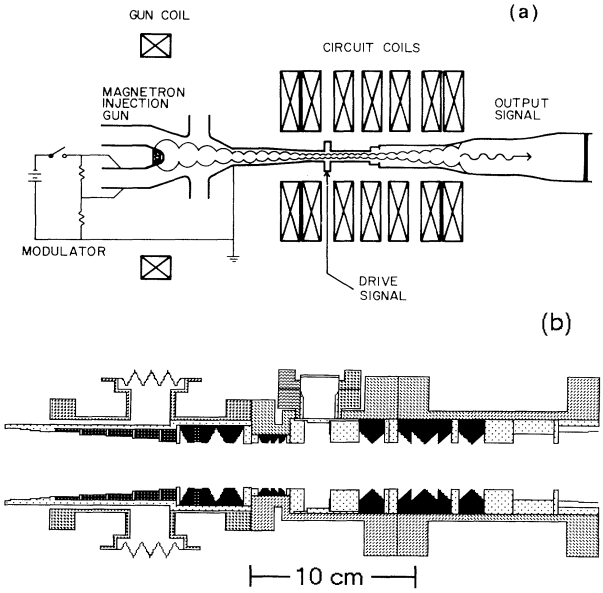

FIG. 1. Schematic of the gyroklystron: (a) overall facility view and (b) two-cavity circuit.

magnetron which is mechanically tunable from 9.7 to 10.0 GHz provides the input power. Amplified power is extracted axially through a coupling aperture in the second cavity and travels through two nonlinear tapered wall sections [16] and the beam dump to a half-wavelength beryllia output window.

Far-field measurements in an anechoic chamber are used to estimate output power and mode purity. A portion of the output signal is sent to an HP 8566B spectrum analyzer to obtain frequency information. The receiving antenna is made from an open-ended section of standard X-band waveguide and can be rotated by 90° and remotely swept radially more than 1 m. The axial separation between the output window and the antenna is approximately 1.13 m. Calibration measurements of the TE_{01} mode pattern agree well with theory. Chamber coupling at the radiation pattern maximum is -33.55 ± 0.35 dB. An additional attenuation of -50.00 ± 0.20 dB is added via rectangular couplers and variable attenuators. Crystal calibration is to within ± 0.15 dB. Absolute power measurements are referenced to a recently recalibrated power meter and relative measurements are performed with a scalar network analyzer. Note that all stated calibration measurements are for 9.87 GHz.

During calorimetry, a mode-selective directional coupler provides the microwave power envelope and gives an additional peak-power estimate. The coupler uses a 0.127-m-diam circular guide as the main arm and a cutdown X-band waveguide as the secondary arm. There are twenty holes of various sizes arranged in a resonant configuration over 0.65 m. The measured TE_{01} coupling is -60.78 ± 0.50 dB and the directionality is better than 25 dB. Suppression of the TE_{11} is theoretically predicted to be better than 20 dB. Additional attenuation of -23.74 ± 0.15 dB is added to get crystal signals into the calibrated range. The calorimeter consists of methanol flowing between two conical polyethylene pieces in a 0.127-m metal pipe. The surface of one of the cones has a spiral groove to improve heating uniformity. Reflections from this nonresonant load are down by 20 dB. The diagnostic hardware is filled with sulfur-hexaflouride because air in the system breaks down at the maximum power level. Microwave heating of the methanol is measured by a thermopile which evaluates the difference in temperature between the fluid entering and exiting the load. The measurement is compared to resistive heating of the methanol *in situ*. Bench-test measurements against a 20-W cw signal in the TE_{01} mode at the proper frequency give good agreement between the calorimeter and the power meter.

An enlargement of the two-cavity circuit is shown in Fig. 1(b). Both theory and previous experiments indicate that TE_{11} modes with frequencies between 7 and 8 GHz pose the greatest spurious oscillation risk. The regions outside the cavities are therefore designed to maximize losses in that range while providing sufficient isolation for the desired mode. The beam tunnel to the left of the input cavity is heavily loaded with aluminum silicate (lossy ceramics are indicated in black) and provides an average single-pass TE_{11} attenuation of 27 dB in that range. The drift section between cavities has a length of 0.109 m and contains eight tapered ceramic rings (80% BeO, 20% SiC). This nonresonant configuration provides a minimum TE_{11} attenuation of 10 dB from 7 to 12.4 GHz and more than 22-dB attenuation at 8 GHz. Attenuation in the TE_{01} mode near 10 GHz is too large to measure. The resonant frequency and quality factor Q for the input cavity are 9.846 ± 0.002 GHz and 214 ± 10, respectively. Part of the input-cavity Q is obtained from losses in a small annular aluminum silicate ring on the sidewall. The resonant frequency and Q for the output cavity are 9.847 ± 0.002 GHz and 224 ± 10, respectively. The output-cavity Q is essentially diffractive. The lengths of the input and output cavities are 0.0173 and 0.0240 m, respectively. To prevent oscillations in modes near cutoff after the output cavity, the output waveguide wall has a 2° taper.

For the experiment, beam voltage is limited to 90% of the design value due to intermittent modulator problems. The drive power is limited to 45 kW as a result of breakdown across the input window surface due to enhanced electric fields near the Kovar sleeve. The achievable velocity ratio α is limited by instabilities as reported elsewhere [15]. Given the nature of the bunching mechanism, it is reasonable to expect that the optimal magnetic fields for energy extraction and bunching are not the same. A careful search of parameter space reveals that an output-cavity field of 0.474 T yields the highest efficiency while an input-cavity field 15% higher yields the highest gain. These fields represent a detuning from the cyclotron frequency of 26.6% in the output cavity and 15.6% in the input cavity. The power is essentially unchanged for voltages in the range 410–440 kV, so 425 kV is used as the nominal operating point. The optimal current is near 150 A. The optimal frequency is nearly 25 MHz above the cold-cavity frequency.

Figure 2(a) reveals the typical time structure of the output power signal at the optimal parameters. Shot-to-shot variations in the output signal are quite small. The data are unfolded from the crystal voltage pulses assuming TE_{01}, 9.87-GHz operation. The solid line represents the measurement from the anechoic chamber. The dashed line represents a result from the directional coupler taken at the same operating point (but several days later). The beam voltage pulse is also displayed as indicated. The peak power is about 20 MW and the power remains above 15 MW for 1 μs. The variation in power is primarily due to relative changes in the control anode voltage compared to the cathode voltage. The lack of adequate capacitive compensation in the resistive divider yields an increase in α towards the end of the pulse. The two spikes between 1.2 and 1.6 μs represent a TE_{11}

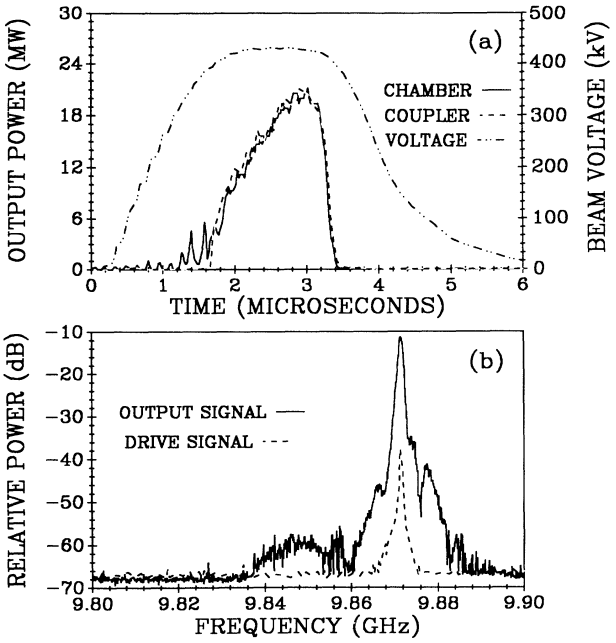

FIG. 2. Power measurements at the optimal parameters: (a) time evolution of amplified pulse and (b) spectra of drive and amplified signals.

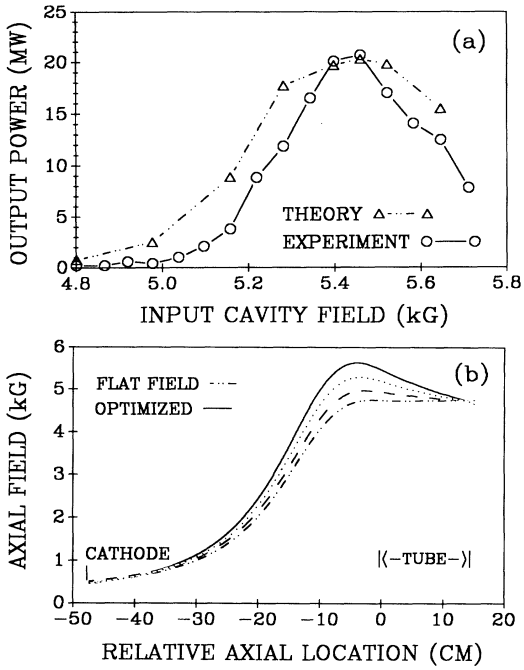

FIG. 3. (a) Peak measured and theoretical output power vs input-cavity axial magnetic field with remaining parameters fixed at optimal values and (b) simulation of axial-field profile on axis.

instability near 7.25 GHz. A comparison of the measured and theoretical angular distribution of radiated power indicates that the instability occurs only on the rise of the voltage pulse and that the remaining microwave energy is purely in the TE_{01} mode. The actual power in the instability is about 10 dB lower than indicated, because of calibration differences between modes and frequencies. These spikes do not appear on the coupler signal because the secondary arm has a cutoff frequency near 8.5 GHz. Power estimates from the methanol calorimetry and from the crystal detector are compared at two flow rates and at pulse repetition rates from 1 to 3 Hz. The detector indicates peak energies of 27 J per pulse. Calorimetry measurements consistently read about 0.5 dB higher. While the calorimetry is probably more accurate, we prefer to quote the more conservative values.

The time-averaged spectrum is shown for the drive and output signals in Fig. 2(b). The peak frequencies of 9.8715 agree to within the resolution of the meter. The drive power at the optimal point is about 44.2 kW, resulting in a gain figure of 26.5 dB. The coupling loss is less than 45%.

For an approximately constant magnetic field in one cavity, the measured output power is a strong function of the field in the other cavity. In Fig. 3(a), for example, measured power is plotted as a function of input-cavity magnetic field with the output-cavity field held at 0.474 T. The strong dependence on field is clearly apparent with a full width at half maximum power of about 7.3%. Results from a simulation that include ac space-charge effects [17] are also shown. The ac space charge acts mainly to enhance the predicted gain of the circuit. Simulated beam parameters are based on results from an electrostatic gun code [18]. Uncertainties in several experimental quantities can lead to systematic uncertainties in α up to $\pm 10\%$ and a similar uncertainty in drive power. Nonetheless, theory predicts the magnitude and location of the maximum output power well and yields a larger, but reasonable, estimate of the half-power points. Because the input power is fixed, the output power levels are not saturated (according to theory) and represent the dependence of gain on experimental parameters.

Calculations of the field profile are shown in Fig. 3(b) for a flat field, for the optimal field, and for two examples in between. Because simulations indicate that the magnetic moment is a well conserved quantity, the figure shows that beams immersed in any of these field profiles will have similar velocity ratios (hence similar perpendicular energies) in the output cavity. Thus, the difference in performance results mostly from the difference in α in the input cavity and the effect on bunching that α entails. For the optimal case, the maximum magnetic compression is 12.3 and computer simulations indicate that $\alpha = 1.15$ at the input-cavity center and $\alpha = 0.98$ at the output-cavity center. These parameters, coupled with the overall efficiency, indicate a conversion of 74% of the perpendicular electron energy into microwave output power (assuming constant axial momentum). In the absence of

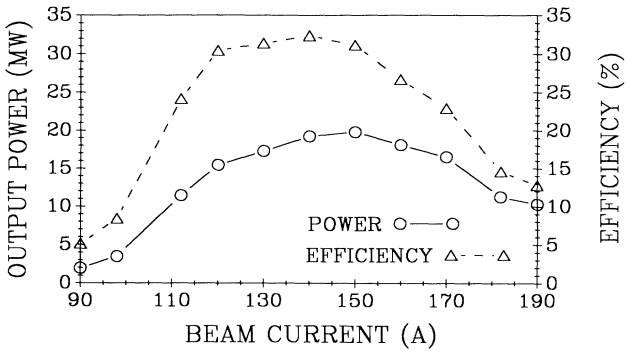

FIG. 4. Efficiency and peak-power measurements as a function of beam current. The other parameters are fixed at optimal values.

rf, the beam quality in the output cavity is estimated by simulations to be $\Delta v_z/v_{z0}=5.3\%$. At the optimal parameters, theory indicates that the beam current is 34% of the start oscillation current (SOC) in the input cavity and 65% of the SOC in the output cavity.

Figure 4 shows peak beam power and total efficiency as a function of beam current. A maximum efficiency of 32% occurs at 140 A. The decrease in power at high currents appears to be caused by several factors. At full current, α is 13% lower than at 150 A so that the perpendicular energy actually decreases slightly. Furthermore, simulations indicate that beam velocity spread increases at higher currents. Finally, since the injected frequency is fixed, beam detuning can have a significant effect. At 110 A, for example, the optimal frequency is 10 MHz lower than the injected frequency.

In summary, 20 MW is produced in a two-cavity gyroklystron operating at 9.87 GHz in the TE_{01} mode with an efficiency of 31% and a gain of 26 dB. Tapering the axial magnetic-field profile is essential to achieve optimal results, as flat-field power levels (for comparable beam powers) are more than 7 times smaller. These results point the way to a new type of rf driver for future multi-TeV linear colliders. Future work will focus on gyroklystrons with intermediate cavities and gyroklystrons at frequencies near 20 GHz.

The authors wish to thank K. Felch and D. Welsh for many useful discussions. We also thank W. Main and S. Tantawi for their contribution to the calorimeter and directional coupler. We appreciate the efforts of D. Reichenthal, M. Naiman, J. Renbaum, M. Skopec, D. Krivitsky, V. Specht, and S. Demske. This work was supported by the U.S. Department of Energy.

[a]Permanent address: Physical Sciences, Inc., Alexandria, VA 22314.

[1] E.g., *Proceedings of the International Workshop on Next-Generation Linear Colliders, Stanford Linear Accelerator Center* (SLAC Report No. 335, 1988).
[2] M. A. Allen *et al.*, Phys. Rev. Lett. **63**, 2472 (1989).
[3] J. Schneider, Phys. Rev. Lett. **2**, 837 (1959).
[4] M. Reiser, W. Lawson, A. Mondelli, and D. Chernin, in *New Techniques for RF Accelerators II,* edited by M. Puglisi, S. Stipcich, and G. Torelli (Plenum, New York, 1989), pp. 65–129.
[5] V. L. Granatstein, M. E. Read, and L. R. Barnett, in *Infrared and Millimeter Waves,* edited by K. Button (Academic, New York, 1982), Vol. 5, pp. 267–304.
[6] K. E. Kreischer *et al.*, Phys. Fluids B **2**, 640 (1990).
[7] K. Felch *et al.*, Proc. SPIE **1514**, 315 (1990).
[8] K. R. Chu, L. R. Barnett, W. K. Lau, L. H. Chang, and H. Y. Chen, IEEE Trans. Electron Devices **37**, 1557 (1990).
[9] W. M. Bollen, A. H. McCurdy, B. Arfin, R. K. Parker, and A. K. Ganguly, IEEE Trans. Plasma Sci. **13**, 417 (1985).
[10] A. C. McCurdy, C. M. Armstrong, W. M. Bollen, R. K. Parker, and V. L. Granatstein, Phys. Rev. Lett. **57**, 2379 (1986).
[11] V. L. Granatstein *et al.*, IEEE Trans. Nucl. Sci. **32**, 3157 (1985).
[12] K. R. Chu, V. L. Granatstein, P. E. Latham, W. Lawson, and C. D. Striffler, IEEE Trans. Plasma Sci. **13**, 424 (1985).
[13] W. Lawson *et al.*, Int. J. Electron. **61**, 969 (1986).
[14] J. P. Calame and W. Lawson, IEEE Trans. Electron Devices **38**, 1538 (1991).
[15] J. P. Calame *et al.*, J. Appl. Phys. (to be published).
[16] W. Lawson, IEEE Trans. Microwave Theory Tech. **38**, 1617 (1990).
[17] P. E. Latham, IEEE Trans. Plasma Sci. **18**, 273 (1990).
[18] W. B. Herrmannsfeldt, SLAC Report No. 226, 1979 (unpublished).